# Sensitivity Pattern of Femtosecond Laser Micromachined and Plasma-Processed In-Fiber Mach-Zehnder Interferometers, as Applied to Small-Scale Refractive Index Sensing

Monika Janik, Anna K. Myśliwiec, Marcin Koba, Anna Celebańska, Wojtek J. Bock, *Life Fellow, IEEE*, and Mateusz Śmietana

***Abstract*— A highly sensitive refractive index (RI) sensor based on an in-fiber Mach–Zehnder interferometer is discussed. The sensor is fabricated by femtosecond laser in a single-mode fiber. A cylindrical cavity is micromachined in the fiber cladding and partly in the fiber core, forming an interferometric structure. We have found that when the spectral response of the structure to RI is considered, a periodic pattern is observed and the sensitivity highly increases with RI and reaches over 23 000 nm/RIU within the RI range of 1.4200—1.4400 RIU. Moreover, during the measurement of cavities with diameters in the order of tens of micrometers, we found the cavity-filling process to be both difficult and time-consuming, especially when high-RI liquids are being investigated. We therefore applied reactive ion etching in oxygen plasma, which significantly changed the wettability of the cavity's surface and enabled fast cavity filling with any investigated liquid. Due to its ultra-high sensitivity and capability for investigating sub-nanoliter volumes of liquids, the sensor could be well suited for chemical and bio-sensing applications.**

***Index Terms*— Mach-Zehnder (MZ) interferometer, microstructure fabrication, laser materials processing, interferometry, optical fiber sensors, reactive ion etching (RIE), refractive index sensing.**

## I. Introduction

THERE is a huge diversity of optical fiber sensors based on, e.g., fiber gratings [1] and interferometers [2]. They differ in their principle of operation, means of fabrication (irradiation, ablation, deposition, splicing, etc.), and geometry. The great variety of optical fiber sensors and their unique properties, such as immunity to electromagnetic interference and the possibility of remote and distributed sensing, often makes them perfect candidates for sensing of many parameters such as temperature, humidity, strain, pressure, and refractive index (RI) [1]–[4], as well as for chemo- and biosensing [5], [6]. In many cases where aqueous solutions need to be examined, e.g., in chemical or biological experiments, only small volumes of analyte are available. Among many other sensing structures micro-cavity Mach-Zehnder interferometers (MZIs) have recently emerged as devices which can meet that challenging demand. There are many traditional methods to fabricate MZIs, but in general, they are not repeatable and the fabricated structures show relatively low RI sensitivity ($10^2 - 10^3$ RIU), as well as operating efficiently only in the high-RI range [7], [8].

Application of femtosecond (fs) laser ablation has many advantages, including negligible heating of the beam-exposed area with extremely short laser pulses and high peak power. It thus causes very little damage in the working area and can produce small, well-defined shapes. Many microchannels and microholes have been fabricated in optical fibers using fs laser micromachining, e.g., [9]–[13]. Some of them operate as fiber in-line interferometers such as: Fabry-Perot interferometers (FPIs) [10]–[12] or Michaelson interferometers (MIs) [13]. Just a few of them were fabricated in one-step fs laser micromachining process, nevertheless the sensitivity of these devices in measurements of changes of RI of water was 1163 nm/RIU at 1550 nm [12]. The majority of the microcavities are fabricated in multistep processes that include very hard to control and hardly repeatable wet etching (in hydrofluoric acid (HF) or other acids etchants) [10], as well as a fusion splicing. Despite the processing the obtained RI sensitivity hardly exceeds 1000 nm/RIU [11].

The fs laser system was also recently used to fabricate several micro-cavity in-line MZI ($\mu$IMZI) structures, which differed in shape, but were all based on a micro-cavity in an optical fiber [14]–[18]. One of the first presented $\mu$IMZIs was based on a V-shape micro-cavity and was post-processed by etching in hydrofluoric acid (HF). The sensitivity of this sensor was about 10,000 nm/RIU within the range between 1.332 and 1.352 RIU [15]. Then Jiang et al. developed a $\mu$IMZI sensor

Manuscript received March 19, 2017; revised April 12, 2017; accepted April 12, 2017. Date of publication April 18, 2017; date of current version May 5, 2017. This work was supported in part by the National Science Centre, Poland under Grant 2014/13/B/ST7/01742, in part by the Canada Research Chairs Program, and in part by the Natural Sciences and Engineering Research Council of Canada (Strategic, Discovery and Industrial Research Grant Programs). The associate editor coordinating the review of this paper and approving it for publication was Dr. Daniele Tosi. *(Corresponding author: Monika Janik.)*

M. Janik, A. Celebańska, and W. J. Bock are with the Centre de Recherche en Photonique, Université du Québec en Outaouais, Gatineau, QC J8X 3X7, Canada (e-mail: monikaa.janik@gmail.com; annacelebanska@gmail.com; wojtek.bock@uqo.ca).

A. K. Myśliwiec and M. Śmietana are with the Institute of Microelectronics and Optoelectronics, Warsaw University of Technology, 00-662 Warsaw, Poland (e-mail: a.debowska@stud.elka.pw.edu.pl; m.smietana@elka.pw.edu.pl).

M. Koba is with the Institute of Microelectronics and Optoelectronics, Warsaw University of Technology, 00-662 Warsaw, Poland, and also with the National Institute of Telecommunications, 04-894 Warsaw, Poland (e-mail: mkoba@elka.pw.edu.pl).

Digital Object Identifier 10.1109/JSEN.2017.2695544

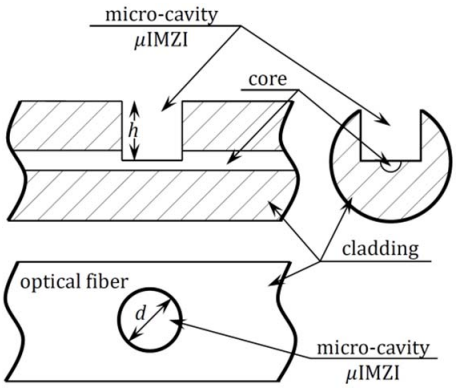


Fig. 1. Schematic drawing of the $\mu$IMZI structure.

with a U-shape structure which exhibited RI sensitivity reaching 3,754.79 nm/RIU with the RI ranging from 1.0001143 to 1.0002187 RIU where gas concentrations can be measured and over 12,000 nm/RIU in the RI range from 1.3330 to 1.3381 RIU for investigation of sucrose solutions [16]. A $\mu$IMZI sensor based on a rectangular cavity structure was also reported [17]. For RI measurement purposes, the structure exhibited RI sensitivity as high as 17,000 nm/RIU within RI values ranging from 1.3371 to 1.3407 RIU. In this case, the spectral response of the device was also fine-tuned by the HF etching process.

For most of the micro-structures their penetration by water-based liquid strongly dependents on the cavity size. Usually it takes up to 15 minutes [4] for a single filling. This disadvantage makes the structures poorly applicable in short-timed or on-site measurements.

In this paper, we present a $\mu$IMZI sensing structure with ultra-high RI sensitivity, which can be obtained in a higher RI range when the periodic character of a spectral response is considered. In contrast to earlier reported works, the proposed structure is fabricated in a circular shape with an fs laser followed by oxygen plasma post-processing. The plasma post-processing, i.e., reactive ion etching (RIE) in oxygen, was used in order to better define the flat and clean bottom of the micro-cavity, and also to improve the hydrophilic properties of its sidewalls. Moreover, the procedure has already been used in post-processing of other fiber sensing structures [19], [20]. It is also known to be accurate, and more precise than any other wet etching process, where removal of the etchant from the cavity is difficult or barely possible to control [17].

## II. Experimental Details

### A. Manufacturing of the $\mu$IMZI Structures

Structures in the form of cylindrical micro-cavities (Fig. 1) were fabricated in standard Corning SMF28 fibers. The cavities have a circular cross-section and flat bottom (diameter, $d$). Their walls (height, $h$) with good approximation are perpendicular to the fiber's long axis.

The micromachining process was done using a Solstice Ti:Sapphire fs laser operating at $\lambda = 795$ nm. The fiber was irradiated by 82 fs pulses. The system was working with a repetition rate of 10 kHz. In order to make the micro-cavity, the laser beam was directed into a suitably designed micromachining setup based on the Newport $\mu$Fab system.

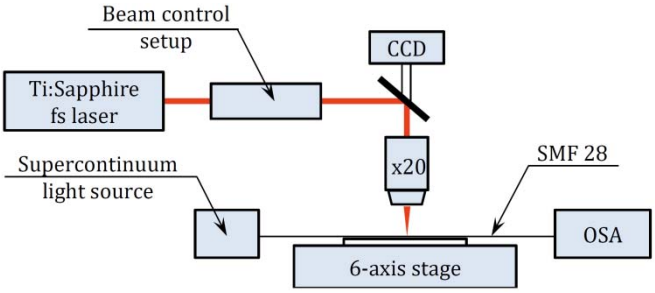


Fig. 2. Scheme of the fs-laser-based micro-fabrication setup.

The system was equipped with a 20× lens, with NA = 0.30. Fiber transmission was monitored during the process with an NKT Photonics SuperK COMPACT supercontinuum white light source and a Yokogawa AQ6370C optical spectrum analyzer. The fabrication process was controlled with software developed in-house. The fabrication setup is schematically shown in Fig. 2.

### B. Plasma Post-Processing

The RIE process was performed using the Oxford PlasmaPro NGP80 system. The plasma process was conducted with an $O_2$ flow of 50 sccm, pressure 100 mTorr and power 100 W. The temperature during the processes was set to 20°C. The $\mu$IMZI sample was placed in the chamber together with an LPG located at the same height and an oxidized silicon wafer ($SiO_2$/Si) as a reference for further tests.

### C. $\mu$IMZI Analysis

The fabricated $\mu$IMZIs were examined using the Olympus LEXT OLS3100 confocal microscope. Next, optical transmission of the $\mu$IMZI was monitored in the spectral range of 1,150-1,650 nm using a Leukos SM30 supercontinuum laser source and a Yokogawa AQ6370B optical spectrum analyzer. The RI sensitivity measurements of the $\mu$IMZIs were performed on specially prepared testing surfaces which allowed for the precise control of the amount of dosed liquid and filling of the micro-cavity. We used as external RI ($n_{ext}$) a set of water/glycerin solutions whose $n_D$ varied in the range of 1.3330-1.4400 RIU. It is worth noting that if the measurements were aimed for a precise refractometer, the dispersion characteristics of $n_{ext}$ should had been taken into account. In the disscused case where every measurement of RI is made with the same device in the same conditions and aimed for the reference tests of the dievices' sensitivity, the values of RI are treated not as absolutes but as references. Thus, the $n_D$ of the solution was measured using a Rudolph J57 automatic refractometer working with $2 \cdot 10^{-5}$ RIU accuracy. Values below $10^{-4}$ RIU shown later in Fig. 5 and 8 were rounded for better readability.

### D. Si/$SiO_2$ Reference Wafers Analysis

The water contact angle on the wafer was measured using a Celestron 5 MP Handheld Digital Microscope Pro with a 1 $\mu$l

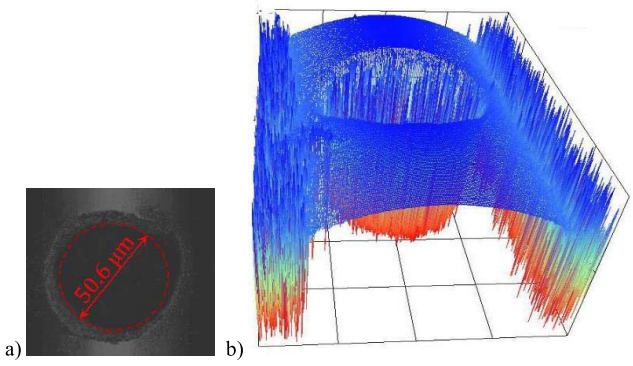


Fig. 3. Microscopic visualization of one of the $\mu$IMZI structures (structure shown here is described in the text as A). The diameter of the red dashed circle shown in a) was assessed in the middle of the micro-cavity's height.

TABLE I
APPROXIMATE DIMENSIONS OF THE THREE INVESTIGATED STRUCTURES

| Sample | A | B | C |
|---|---|---|---|
| **diameter [µm]** | 50.6 | 54.2 | 65.2 |
| **volume [pL]** | 10.9 | 14.1 | 20.6 |
| **height [µm]** | 68 | 68 | 70 |

water droplet (10 seconds after deposition). The value was averaged from five measurements. The measurements were repeated after 24, 48, 72 hours, 1 week, and 2 weeks of storage of the samples in the air. In order to compare the impact on the wettability of the oxygen-plasma and HF post-processing, evaluation measurements were performed for samples etched for 2 minutes in 5% aqueous solution of HF acid. Finally, possible changes in thickness of the $SiO_2$ layer induced by the RIE process were investigated using a Horiba Jobin-Yvon UVSEL spectroscopic ellipsometer following the procedure reported in [20].

## III. RESULTS AND DISCUSSION

### A. Physical Properties of the Investigated $\mu$IMZI

Three structures were chosen to illustrate the high sensitivity capabilities of the proposed $\mu$IMZI. Their dimensions are shown in Table 1. Images showing a top view and a scan through the $\mu$IMZI are depicted in Fig. 3.

It can be seen that, depending on the structure, a volume of liquid in the micro-cavity as small as 11 pL can be investigated. It must be noted that values shown for the height of the cavity are not precise, due to the very rough surface of the bottom and the difficulty of removing the tiny glass shards created by the micromachining process.

### B. RI Sensing With $\mu$IMZI

The transmission spectra of sample C with the RI in the micro-cavity varying from 1.3350 to 1.3600 RIU are shown in Fig. 4a. Both the transmitted power and the central wavelength of the minima change with increasing RI, i.e., they deepen and blue-shift, respectively. Each of the three structures displays multiple minima with free spectral range (FSR) of

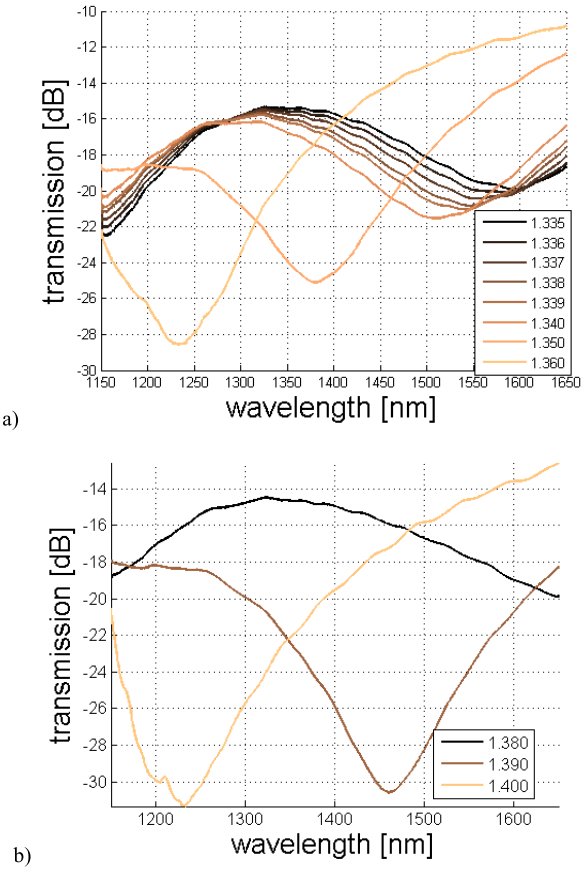


Fig. 4. Transmission spectra of $\mu$IMZI micro-cavity filled with water solutions with different values of RI ranging from (a) 1.33-1.36 and (b) 1.38-1.40 RIU.

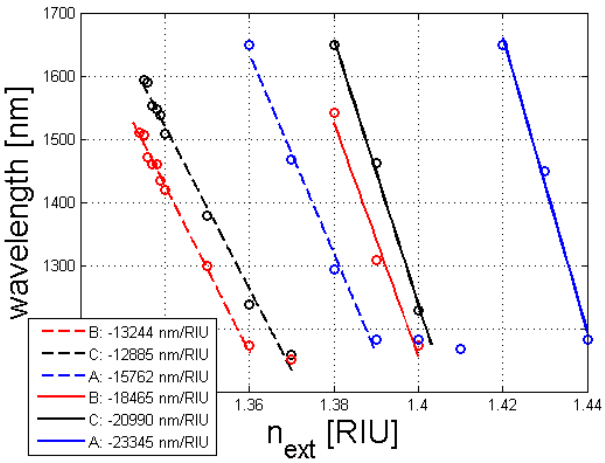


Fig. 5. Sensitivities of the three investigated $\mu$IMZI structures, where the first and second set of minima are marked with dashed and continuous lines, respectively.

over 500 nm. This property makes these structures convenient for sensing purposes. When the RI is further increased, a second minimum can be observed, which also experiences a similar change to the one observed at lower RI (Fig. 4b).

In Fig. 5, the spectral locations of minima are plotted vs RI in the cavity for samples A, B, and C. The points corresponding to each sample are linearly approximated with the least squares method, and the values of sensitivity in different

RI regions are obtained. It is noticeable that the deviation of points from approximation lines is small or negligible which in turn reveals the high linearity of RI sensitivity of the samples. It is also noticeable that the sensitivity is higher for higher RI solutions.

In general, as described, e.g., in [17], the interference intensity in $\mu$IMZI can be expressed by the two-beam interference equation:

$$I = I_1 + I_2 + 2\sqrt{I_1 I_2}\cos\varphi, \tag{1}$$

where the phase difference is given by:

$$\varphi = \frac{2\pi d \Delta n_{eff}}{\lambda} + \varphi_0. \tag{2}$$

In equation (2), $d$ is the MZI diameter (shown in Fig. 1), $\lambda$ denotes the wavelength of a minimum, $\varphi_0$ is an initial phase, and $\Delta n_{eff} = n_{eff}^{co} - n^{cl}$ comprises the effective RI of the remaining part of the fiber core $n_{eff}^{co}$ and that of the circular cavity $n^{cl}$. According to equations (1) and (2), the interference fringe pattern has minima for every odd multiple of $\pi$:

$$\frac{2\pi d \Delta n_{eff}}{\lambda_m} + \varphi_0 = (2m+1)\pi, \tag{3}$$

which can be transformed into:

$$\lambda_m = \frac{2\pi d \Delta n_{eff}}{(2m+1)\pi - \varphi_0}, \tag{4}$$

which defines $\lambda$ for every minimum.

As can be seen from equation (4) the increase in $n_{ext}$, which in this case corresponds to the RI in the circular microcavity $n^{cl}$, causes an increase of $n_{eff}^{co}$ and at the same time a decrease of $\Delta n_{eff}$. The growth of $n_{eff}^{co}$ is much slower than the decrease of $\Delta n_{eff}$ and consequently $\lambda_\mathrm{m}$ decreases. This behavior is experimentally observed and shown in Fig. 5. Further, the sensitivity of the structure ($S_m$) may be expressed as:

$$S_m = \frac{d\lambda_m}{dn_{ext}} = \frac{2\pi d}{(2m+1)\pi - \varphi_0}\left(\frac{dn_{eff}^{co}}{dn_{ext}} - \frac{dn^{cl}}{dn_{ext}}\right), \tag{5}$$

where $n_{ext}$ is the value of the RI of the examined liquid solution, which in the case under discussion may be assumed as $n_{ext} = n^{cl}$. Such approximation is valid since the liquid covers the whole area of the cavity. The key term $dn_{eff}^{co}/dn_{ext}$ in equation (5) is responsible for sensitivity increase at higher RI solution values. At this point, it is necessary to realize that the effective $n_{eff}^{co}$ is an increasing function of $n^{cl}$, or equally $n_{ext}$. This means that the increase in $n_{ext}$ will cause an increase in $S_m$, especially for higher values of RI, for which $n_{eff}^{co}$ tends to its maximal value. This phenomenon is experimentally confirmed and shown in Figs. 5 and 6.

To our best knowledge, the highest RI sensitivity of a $\mu$IMZI was reported in [17] and reached 17,197 nm/RIU in the range between 1.3371 and 1.3407 RIU. The $\mu$IMZI structures presented in this paper display sensitivities from approximately 12,000 ($n_D$ between 1.3330 and 1.3600 RIU) to over 23,000 nm/RIU ($n_D$between 1.4200 and 1.4400 RIU), the highest ever reported for a $\mu$IMZI structure to date.

It is evident from Fig. 6 that the proposed $\mu$IMZI structure covers a wide range of RI values of aqueous solutions and thus

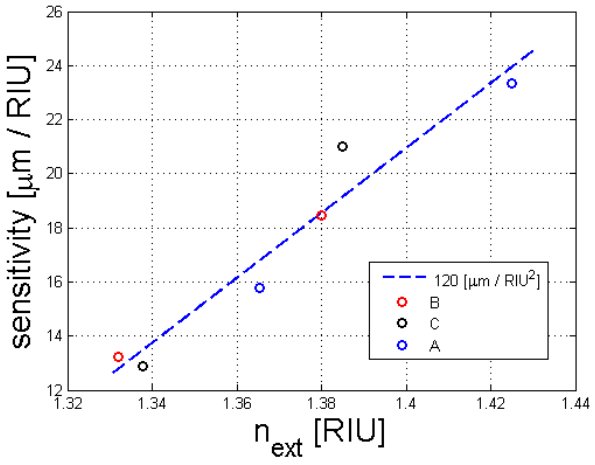


Fig. 6. The absolute value of sensitivity at $\lambda = 1550$ nm plotted against external RI. The linear approximation of these points describes the relationship between the $S_m$ and $S_{m+1}$ sensitivities.

offers interesting capabilities in various sensing applications. The sensitivity clearly increases with RI (Fig. 6). The results stay in agreement with [16], where the sensitivity for RI close to 1 and 1.3330 RIU was over 3,000 and 12,000 nm/RIU, respectively. As shown in this work, the trend is also sustained for higher RI. Furthermore, it is worth noting that through proper design of the structure's parameters, such as diameter or height, the sensing range can be tuned to the desired RI range. Moreover, taking into consideration the reported results on temperature cross-sensitivity of previously presented similar MZI structure [21], where none or negligible temperature sensitivity was shown, we assume similar low-temperature senistivity effect for the presented $\mu$IMZI.

### C. Effect of $O_2$ Plasma Processing

Our further investigation incorporated plasma etching as a method of improving the sensing capabilities of the $\mu$IMZI. The plasma etching depends on the etched material and corresponding process parameters, including the composition of the gasses and power of the RF generator [22]. It had been shown that the process is highly selective, specifically, the $O_2$ etching of $SiO_2$ is negligible [20]. Thus the $SiO_2$/Si wafer was a good reference substrate for $O_2$ plasma etching. For each test, the $SiO_2$/Si slide, and an LPG were reference samples in the process. The LPG was assumed to be a good reference for observing the etching effect due to the fact that it had been induced in the same fiber as $\mu$IMZI and it was proven to be highly sensitive to variation in cladding thickness [19], [20]. The transmission spectra in water before and after etching for both the samples are shown in Fig. 7.

The samples underwent two consecutive etching processes in $O_2$ plasma, where the first process lasted for 6 minutes and the second one 3 minutes. Comparison of Fig. 7a and 7b reveals that the etching has an influence on the spectral response of the LPG (Fig. 7b) but very little influence in the case of the $\mu$IMZI (Fig. 7a) in terms of minima shift. Looking at the LPG, a small shift of the observed resonance towards a longer wavelength can be seen after each etching process (Fig. 7b). The spectral response of the LPG confirms slight modification of the fiber cladding induced by plasma.

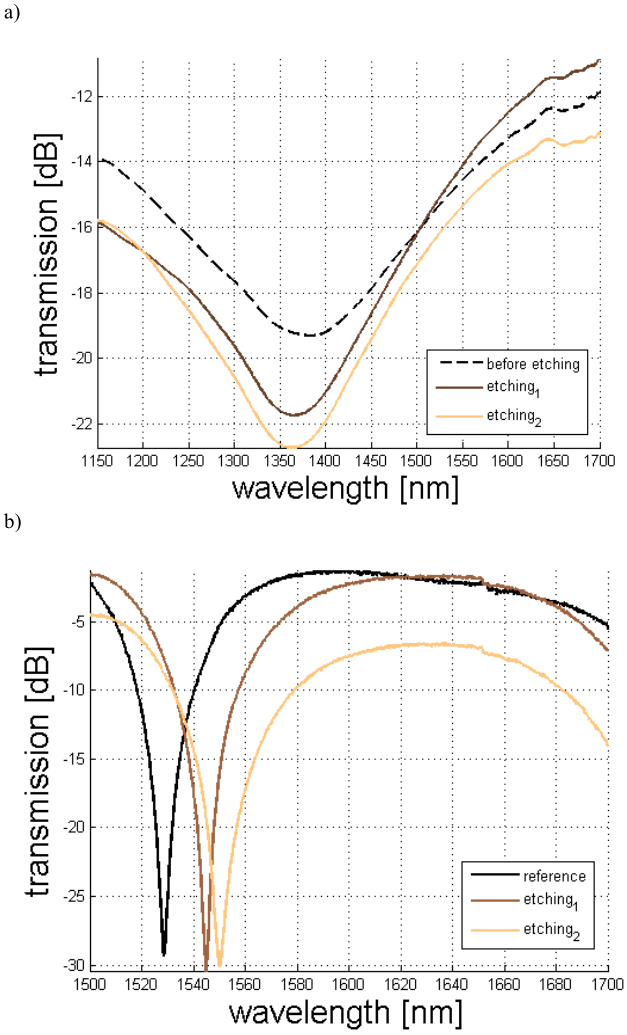


Fig. 7. Effect of each etching process on transmission spectra for a) a $\mu$IMZI micro-cavity and b) an LPG.

It must be noted here that the etching was unmeasurable when the reference $SiO_2$/Si wafers were investigated using spectroscopic ellipsometry. The result (Fig. 7b) confirms that there is possible etching of the fiber cladding by $O_2$ plasma, but it is only visible when devices as sensitive as LPGs are applied [20].

As seen in Fig. 7a, the processes improved smoothness of the spectra. The spectrum behaves in the same way as after wet etching, which cleans all remaining material from the inside of the microcavity [17]. Knowing the nature of the plasma-based processes and considering the results of the wet etching effect, we can assume that the improved smoothness of the spectrum is caused by the appearance of two main processes: firstly the unevenly crafted bottom of the micro-cavity is being made flat, and secondly the sidewalls of the micro-cavity are being made even and any remaining glass shards are being removed. After both $O_2$ plasma etching processes the $\mu$IMZI sample was measured again in the RI range 1.33-1.39. The sensitivity curves before and after etching are compared in Fig. 8.

The plot shows comparable values for both the analyzed cases, revealing that although the process affected the spectra, it had no significant impact on the overall sensitivity. Based on

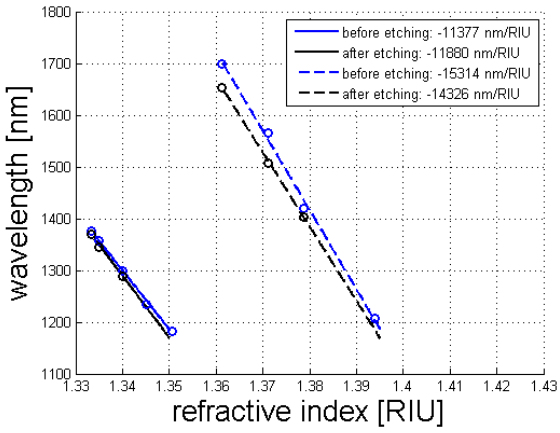


Fig. 8. Sensitivity of the investigated $\mu$IMZI structure before and after $O_2$ plasma etching.

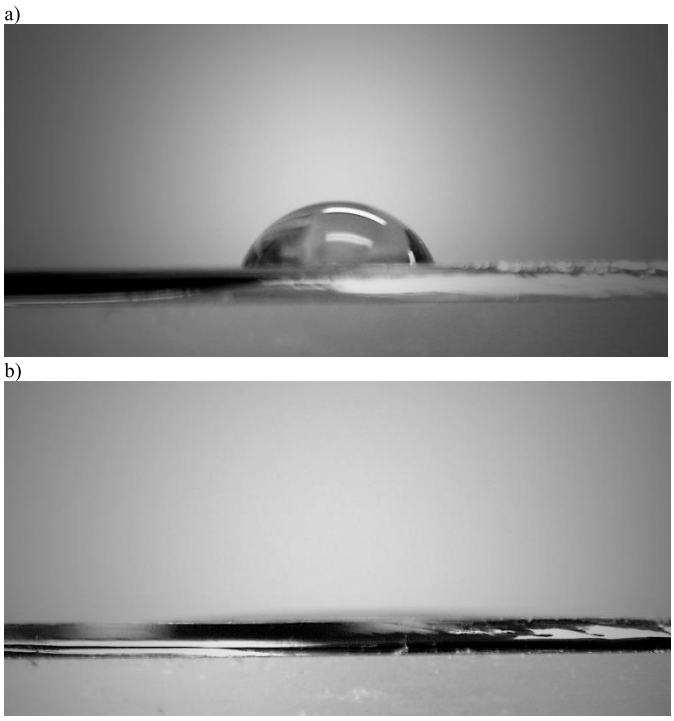


Fig. 9. Effect of $O_2$ etching process on $SiO_2$ surface properties: a) before (contact angle is equal to 64°) and b) after (contact angle is unmeasurable because of high wettability).

this result, we can conclude that the plasma-based etching used on micro-cavities has the advantage of highly precise post-processing, which cleans and smoothes the cavity area. Moreover, it might be used as a gentle and highly controlled chemical etching. Chemical etching is very hard to use in extremely rapid or short processes, where e.g. HF acid before being completely washed from the micro-cavity causes further, generally unwanted, etching.

### *D. Surface Properties of the Micro-Cavity*

Because of its very small size, the micro-cavity can be problematic to investigate. The biggest challenge is definitely the process of filling it with liquids, especially those with high RI. The micro-cavity must not only be cleaned after

fabrication, but good wettability of its inner surface must be assured. We found that the surface inside the micro-cavity after treatment with $O_2$ plasma became very hydrophilic, which was confirmed via separate viscosity tests on accompanying *$SiO_2$/Si* reference wafers. Fig. 9 shows the changes in the water contact angle before and after the $O_2$ etching process.

As a result of the etching process, the contact angle was unmeasurable due to very high hydrophilicity of the surface (Fig. 9b). This made it possible to easily introduce the sample liquid into the micro-cavity, facilitating measurement of liquids with higher RI or high viscosity. The time which takes the liquid to fully fill the cavity is strongly dependent on its properties, such as size and shape. Before the plasma processing it took usually around 12-15 minutes for the high-viscosity liquids to fill the cavity. After plasma treatment, the filling the cavity was immediate independently of the cavity size and liquid viscosity.

When compared to the HF-processed $SiO_2$ samples, the plasma-processed samples, both stored in ambient air, had lower stability during the 2 weeks of storage. However, within 24 hours after etching, the wettability of samples was comparable. An advantage of the $O_2$ plasma treatment is that is it environmentally friendly and eliminates the use of HF, a hazardous and highly toxic chemical.

## IV. Conclusions

In this paper, we demonstrate the ultra-high RI sensitivity of a cylindrically-shaped micro-cavity in-fiber MZI, which was fabricated solely with a femtosecond laser. An interferometric pattern has been observed, where each minima appearing at higher RI shows higher RI sensitivity. The effect has been explained theoretically and shown experimentally. The sensitivity of the sensor reached 23,345 nm/RIU for aqueous solutions of glycerin ranging from 1.4200 to 1.4400 RIU, which is the highest reported value to the date for this type of sensor. Moreover in this work, in contrast to previously presented studies utilizing chemical etching, we also demonstrated an application of $O_2$-based RIE for micro-cavity inner surface cleaning and increase in surface wettability. The treatment allows for fast introduction of the liquid into the micro-cavity. Due to its ultra-high sensitivity, the sensor might well prove suitable for future applications where sub-nanoliter volumes are investigated.

## References


[1] M. Śmietana, M. Koba, P. Mikulic, and W. J. Bock, "Towards refractive index sensitivity of long-period gratings at level of tens of $\mu$m per refractive index unit: Fiber cladding etching and nano-coating deposition," *Opt. Exp.*, vol. 24, no. 11, pp. 11897–11904, May 2016.

[2] Y. Wang, M. Yang, D. N. Wang, S. Liu, and P. Lu, "Fiber in-line Mach–Zehnder interferometer fabricated by femtosecond laser micromachining for refractive index measurement with high sensitivity," *J. Opt. Soc. Amer. B, Opt. Phys.*, vol. 27, no. 3, pp. 370–374, Mar. 2010.

[3] F. J. Arregui, I. R. Matias, K. L. Cooper, and R. O. Claus, "Simultaneous measurement of humidity and temperature by combining a reflective intensity-based optical fiber sensor and a fiber Bragg grating," *IEEE Sensors J.*, vol. 2, no. 5, pp. 482–487, Oct. 2002.

[4] M. Najari, A. M. Javan, and N. Amiri, "Hybrid all-fiber sensor for simultaneous strain and temperature measurements based on Mach–Zehnder interferometer," *Optik-Int. J. Light Electron Opt.*, vol. 126, no. 19, pp. 2022–2025, May 2015.

[5] Y. Chiniforooshan, J. Ma, W. J. Bock, W. Hao, and Z. Y. Wang, "Corrugated fiber grating for detection of lead ions in water," *J. Lightw. Technol.*, vol. 33, no. 12, pp. 2549–2553, Jun. 15, 2015.

[6] M. Koba *et al.*, "Bacteriophage adhesin-coated long-period grating-based sensor: Bacteria detection specificity," *J. Lightw. Technol.*, vol. 34, no. 19, pp. 4531–4536, Oct. 1, 2016.

[7] J. H. Lim, H. S. Jang, K. S. Lee, J. C. Kim, and B. H. Lee, "Mach–Zehnder interferometer formed in a photonic crystal fiber based on a pair of long-period fiber gratings," *Opt. Lett.*, vol. 29, pp. 346–348, 2004.

[8] T. Wei, X. Lan, and H. Xiao, "Fiber in line core-cladding-mode Mach–Zehnder interferometer fabricated by two-point $CO_2$ laser irradiations," *IEEE Photon. Technol. Lett.*, vol. 21, no. 10, pp. 669–671, May 15, 2009.

[9] D. Donlagic, "All-fiber micromachined microcell," *Opt. Lett.*, vol. 36, no. 16, pp. 3148–3150, Aug. 2011.

[10] S. Pevec and D. Donlagic, "High resolution, all-fiber, micro-machined sensor for simultaneous measurement of refractive index and temperature," *Opt. Exp.*, vol. 22, no. 13, pp. 16241–16253, Jun. 2014.

[11] C. R. Liao, T. Y. Hu, and D. N. Wang, "Optical fiber Fabry–Perot interferometer cavity fabricated by femtosecond laser micromachining and fusion splicing for refractive index sensing," *Opt. Exp.*, vol. 20, no. 20, pp. 22813–22818, Sep. 2012.

[12] T. Wei, Y. Han, Y. Li, H. L. Tsai, and H. Xiao, "Temperature-insensitive miniaturized fiber inline Fabry–Perot interferometer for highly sensitive refractive index measurement," *Opt. Exp.*, vol. 16, no. 8, pp. 5764–5769, Apr. 2008.

[13] L. Yuan *et al.*, "Fiber inline Michelson interferometer fabricated by a femtosecond laser," *Opt. Lett.*, vol. 37, no. 21, pp. 4489–4491, Nov. 2012.

[14] L. Zhao *et al.*, "A high-quality Mach–Zehnder interferometer fiber sensor by femtosecond laser one-step processing," *Sensors*, vol. 11, no. 1, pp. 54–61, Dec. 2011.

[15] X. Sun *et al.*, "A robust high refractive index sensitivity fiber Mach–Zehnder interferometer fabricated by femtosecond laser machining and chemical etching," *Sens. Actuators A, Phys.*, vol. 230, pp. 111–116, Jul. 2015.

[16] L. Jiang, L. Zhao, S. Wang, J. Yang, and H. Xiao, "Femtosecond laser fabricated all-optical fiber sensors with ultrahigh refractive index sensitivity: Modeling and experiment," *Opt. Exp.*, vol. 19, no. 18, pp. 17591–17598, Aug. 2011.

[17] X.-Y. Sun *et al.*, "Highly sensitive refractive index fiber inline Mach–Zehnder interferometer fabricated by femtosecond laser micromachining and chemical etching," *Opt. Laser Technol.*, vol. 77, pp. 11–15, Mar. 2016.

[18] Y. Hu, Y. Wang, C. R. Liao, and D. N. Wang, "Miniaturized fiber in-line Mach–Zehnder interferometer based on inner air cavity for high-temperature sensing," *Opt. Lett.*, vol. 37, no. 24, pp. 5082–5084, Dec. 2012.

[19] M. Śmietana, M. Koba, P. Mikulic, and W. J. Bock, "Tuning properties of long-period gratings by plasma post-processing of their diamond-like carbon nano-overlays," *Meas. Sci. Technol.*, vol. 25, no. 11, p. 114001, Oct. 2014.

[20] M. Śmietana, M. Koba, P. Mikulic, and W. J. Bock, "Measurements of reactive ion etching process effect using long-period fiber gratings," *Opt. Exp.*, vol. 22, no. 5, pp. 5986–5994, Mar. 2014.

[21] T. Y. Hu and D. N. Wang, "Optical fiber in-line Mach–Zehnder interferometer based on dual internal mirrors formed by a hollow sphere pair," *Opt. Lett.*, vol. 38, no. 16, pp. 3036–3039, Aug. 2013.

[22] J. W. Coburn and H. F. Winters, "Plasma etching: A discussion of mechanisms," *J. Vac. Sci. Technol.*, vol. 16, no. 2, pp. 391–403, Mar. 1979.



**Monika Janik** received the B.Sc. and M.Sc. degrees in biotechnology from the Wroclaw University of Technology, Poland, in 2014 and 2015, respectively. She is currently pursuing the Ph.D. degree with the Université du Québec en Outaouais, Canada. Her main activities are focused on fiber-optic biosensors for bacterial detection.

**Anna K. Myśliwiec** received the B.Sc. degree in electronics from the Warsaw University of Technology in 2013, where she is currently pursuing the Ph.D. degree. In 2014, she received a Diamentowy Grant from the Polish Ministry of Science and Higher Education.

**Marcin Koba** received the M.Sc. degree in optoelectronics and the Ph.D. degree in electronics from the Warsaw University of Technology, Warsaw, Poland, in 2006 and 2011, respectively. His current interests include laser physics, solid-state physics, optical communication, photonics, fiber-optic sensing structures, and metrology.

**Anna Celebańska** received the M.Sc. degree in chemistry from the University of Warsaw, Poland, in 2009, and the Ph.D. degree in chemistry from the Institute of Physical Chemistry, Polish Academy of Science, Poland, in 2016. Since 2016, she has been a Post-Doctoral Fellow with the Université du Québec en Outaouais, Canada. Her current interests include aptamer- and bacteriophage-based biosensors.

**Wojtek J. Bock** (LF'17) received the M.Sc. degree in electrical engineering and the Ph.D. degree in solid-state physics from the Warsaw University of Technology, Poland, in 1971 and 1980, respectively. Since 1989, he has been a Full Professor of Electrical Engineering with the Université du Québec en Outaouais (UQO), Canada. He is currently the Director of the Photonics Research Center, UQO. He has recently been awarded the SPI-NSERC Senior Industrial Research Chair in Photonic Sensing Technologies for Safety and Security Monitoring. He has authored or co-authored more than 400 scientific papers, patents, and conference papers in the fields of fiber optics and metrology which have been cited about 3500 times. His current research program centers around developing a variety of novel fiber-optic device solutions and sensing techniques with a view to acquiring better performing photonic sensing components, devices and systems for applications in sectors of the national importance to Canada.

Dr. Bock was the Chairman of the International Optical Fiber Sensor Conference (OFS21) held in Ottawa in 2011. He was an Associate Editor of the IEEE/OSA JOURNAL OF LIGHTWAVE TECHNOLOGY and the *International Journal of Sensors*.

**Mateusz Śmietana** received the B.Sc., M.Sc., Ph.D., (Hons.) and D.Sc. degrees in electronics from the Warsaw University of Technology (WUT), Poland, in 2000, 2002, 2007, and 2014, respectively. He was a Post-Doctoral Fellow with Virginia Tech, USA, and the Université du Québec en Outaouais, Canada. Since 2015, he has been an Associate Professor with the Institute of Microelectronics and Optoelectronics, WUT. He has authored or co-authored more than 100 scientific papers. His fields of interest are fiber-optic sensors and thin films.